Evaluation and Comparison of Simulated Electric Field Differences Using Three Image Segmentation Methods for TMS

Tayeb Zaidi and Kyoko Fujimoto

1 Introduction

Magnetic and electrical brain stimulation therapies are widely used to treat neurodegenerative disorders. One of the commonly used non-invasive techniques is transcranial magnetic stimulation (TMS) that employs magnetic induction to stimulate the brain to improve symptoms for diseases such as depression. Computational modeling has been used to assess the effectiveness and safety of TMS. A detailed brain model is available to allow for these assessments [5]; however, the model is only based on one subject. In order to allow for careful planning of a given treatment regimen, modeling needs to be completed on a per-patient basis.

A patient-specific brain model can be created using medical imaging data. Magnetic Resonance Imaging (MRI) structural data is often used for such purpose. There are a variety of semi-automatic segmentation methods available [1, 2, 4, 22] that can generate a 3D head model using a set of T_1- and T_2-weighted images. Segmentation varies across different methods [6, 18]. Therefore, it may affect electric field distributions in electric-field modeling. Some of the segmentation methods resulted in differences in electric field distributions of up to 30% when evaluated with one computational modeling method [11]. More investigations are needed to confirm the degree of differences among different image segmentation and computational modeling methods.

In this study, the T_1- and T_2-weighted images of 16 subjects were processed with three different segmentation methods. Computational modeling of TMS was performed based on each segmented data by targeting both the primary motor cortex and the dorsolateral left prefrontal cortex (DLPFC), then the simulated electric field results were compared and evaluated.

T. Zaidi · K. Fujimoto (✉)
Center for Devices and Radiological Health, US Food and Drug Administration, Silver Spring, MD, USA

S. Makarov et al. (eds.), *Brain and Human Body Modelling 2021*,
https://doi.org/10.1007/978-3-031-15451-5_5

2 Materials and Methods

2.1 MRI Data and Segmentation

MRI T_1- and T_2-weighted images were used from 16 Human Connectome Project healthy subjects [19] with an isotropic resolution of 0.7 mm per voxel. Two pipelines implemented in the SimNIBS software package v3.2 [15] were used for segmentation, *headreco* [10] and *mri2mesh* [20], as well as a highresolution FreeSurfer [2] pipeline (*fshires*) [21]. Both the *headreco* and *mri2mesh* segmentation methods generate surface and volume segmentation of brain and head structures including gray matter (GM), white matter (WM), cerebrospinal fluid (CSF), skull, and skin. The *fshires* pipeline produces GM and WM segmentation based on the native submillimeter resolution.

The surface meshes were generated using the default options from SimNIBs for both *headreco* and *mri2mesh* and the high resolution option within Freesurfer (*fshires*) using the *-hires* flag. The default surface resolution yields surface meshes containing a combined total of roughly 800,000 to 1 million facets.

2.2 Electromagnetic Simulation

A boundary element fast multipole method (BEM-FMM) solver was used for electromagnetic modeling [7–9]. The solver utilizes the generated surface meshes for field estimation. A figure-eight TMS coil was modeled with a diameter of 90 mm for each loop. The coil model was modeled based on a commercial coil (MRiB91 of MagVenture, Denmark). The coil was placed to target both the patient's left primary motor cortex (the hand knob) and the DLPFC via a projection approach and sulcus-aligned mapping [3, 12]. These regions were chosen because they are common targets for TMS therapy. An example positioning of the coil is shown in Fig. 1. Two target points were used for each subject, located within the primary motor cortex and the DLPFC, respectively. The coil position was determined using three steps. First, the coil was placed so that the centerline (shown as the black line in Fig. 1) passed through the given target point on the gray matter interface. Second, the coil centerline was made to be perpendicular to the skin surface. Lastly, the coil position was adjusted so that the dominant field direction was roughly perpendicular to the nearest sulci [7].

2.3 Analysis

Average surface displacement between mesh surfaces generated based on the *headreco* and *mri2mesh* segmentation methods were compared across the 16 subjects for the gray matter, white matter and CSF surfaces. The displacement was calculated by

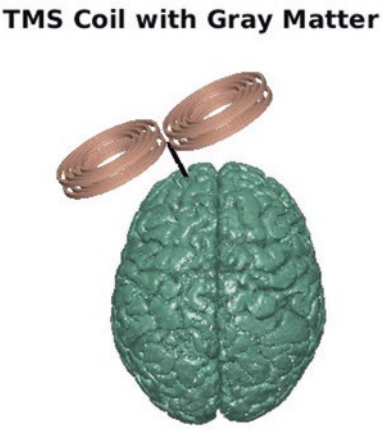

Fig. 1 An example placement of the TMS coil targeting the subject's left motor cortex is shown. The black line (the coil axis) was used to confirm the coil placement and runs perpendicular to the coil

taking the mean of the shortest distance from every triangle centroid of the relevant surface from one segmentation method to all triangle centroids of the surface from the other segmentation method. The electric field values were compared by extracting the values in a 100 mm line perpendicular to the TMS coil axis, along the black line shown in Fig. 1. Comparisons were performed in pairs between *mri2mesh* and *headreco* and between *mri2mesh* and *fshires*. These values were extracted for both of the target points for each subject. The average electric field difference, maximum absolute difference, and maximum percentage difference were compared for all 16 subjects. The average field differences at the target point for both the motor cortex and DLPFC were tested for statistical significance using a paired t-test.

Finally, for additional visualization of the electric field stimulation mapping, all subject electric field results were mapped onto the inflated surface from the FreeSurfer common space (*fsaverage*). The electric field was exported and mapped onto this common surface to map average electric field and its difference surface over the 16 subjects. These maps allow for the qualitative evaluation of focality variations between three different segmentation methods over the entire subject space.

3 Results

All extracerebral and cortical surfaces were successfully reconstructed using the three segmentation methods. The average surface displacement was only calculated for regions of the brain located in the superior cerebral cortex for all 16 subjects between *headreco* and *mri2mesh* and the results are summarized in Fig. 2. The displacement between *fshires* and *mri2mesh* were not compared as the surfaces use the same algorithm from FreeSurfer and the comparison was done by other study [21]. The CSF surface displacement was three times more than the white matter surface displacement, with an average difference of 0.9 mm (±0.2 mm) for the CSF and 0.3 mm (±0.06 mm) for the white matter. An example of all the surfaces overlaid on a subject T_1-weighted image is shown in Fig. 3.

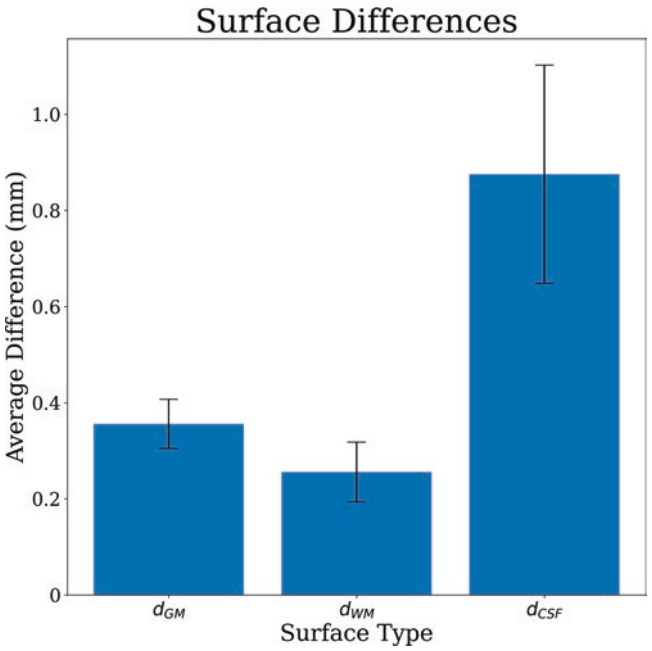

Fig. 2 Average displacement between *headreco* and *mri2mesh* surfaces in millimeters across all 16 subjects for CSF, GM, and WM

For the target point located in the motor cortex, the electric fields showed similar distributions for the *mri2mesh* and the *headreco* segmentation methods. There was an average difference in magnitude of 0.8 V/m and a maximum difference of 61 V/m. The average percentage difference was 2%. In the region of interest within 5 mm of the target point, the average percentage difference was approximately 5%. For the *mri2mesh* and *fshires* segmentation methods, the average percentage difference in the region of interest surrounding the target point was 0.7%. Extracted electric fields (along the dotted line) and the surface contour lines are shown on the subject's T_1 image in Fig. 3.

For the target point located in the DLFPC, there was an average difference of 0.8 V/m in magnitude and a maximum difference of 50 V/m between the *mri2mesh* and *headreco* segmentation methods. The average percentage difference was 2.8%.

Fig. 3 (continued) field results and the thin contours show the *headreco* field results (*fshires* contours are not shown because they are almost identical to the *mri2mesh* results). Color indications for surfaces are red for skin, orange for skull, yellow for CSF, cyan for gray matter, and purple for white matter. The dotted white line on the axial cross section is a projection onto the XY plane of the 100 mm line running along the axis perpendicular from the coil. The electric field result along the dotted white line was extracted as shown at the bottom of the figure. The dotted black line indicates the location of the target point of stimulation. The field peaks were observed at the anatomical structure transition points (represented by arrows): (1) Skin-Skull, (2) Skull-CSF, (3) CSF-GM, (4) GM-WM

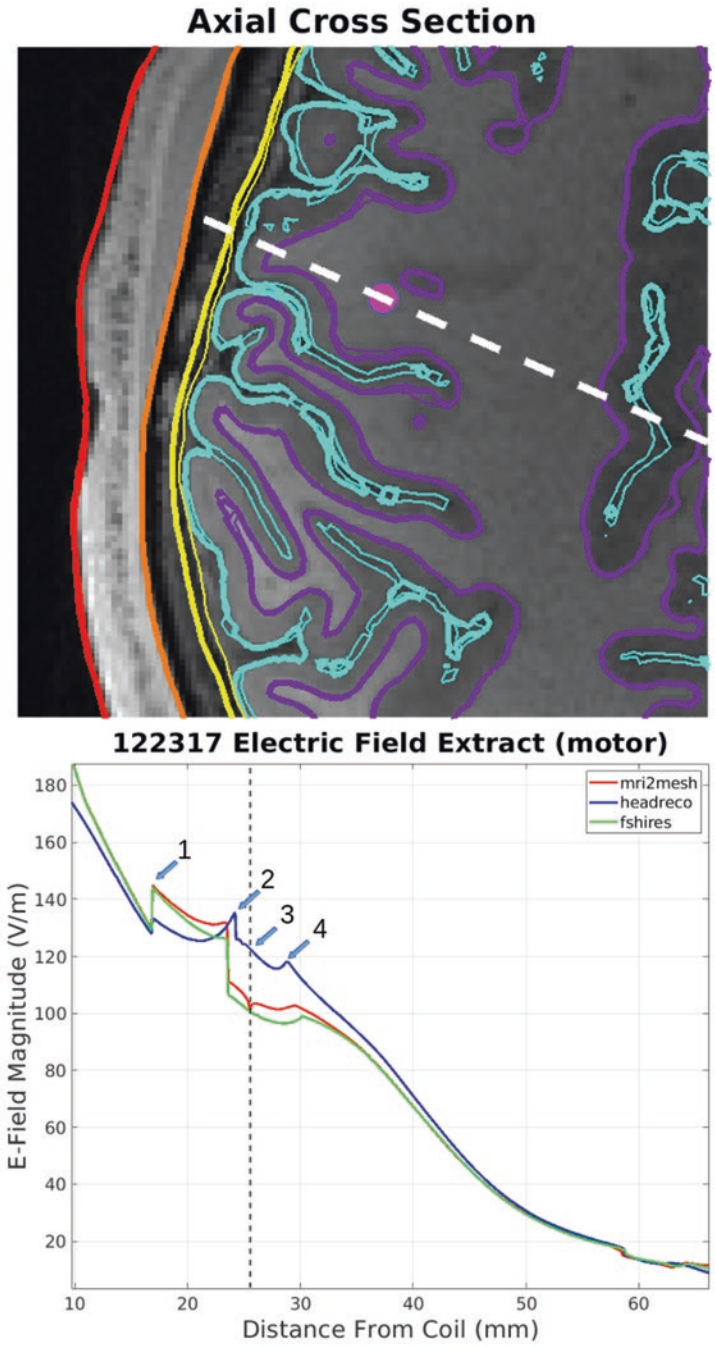

Fig. 3 Example of electric field targeted on motor cortex is shown along with an axial cross section of a subject (target stimulation point in magenta). The thick contours show the *mri2mesh* field

In the region of interest within 5 mm of the target point, the average percentage difference was approximately 1.8%. For the *mri2mesh* and *fshires* segmentation comparison, the average percentage difference in the region of interest surrounding the target point was 0.1%. Extracted electric fields (along the dotted line) and the surface contour lines are shown on the subject's T_1 image in Fig. 4.

The electric field difference across all 16 subjects at the target point between *headreco* and *mri2mesh* was statistically significant ($p = 0.005$) for the motor cortex and not significant between *mri2mesh* and *fshires* ($p = 0.83$). The electric field difference at the target point for the DLFPC was not significant for either the comparison between *mri2mesh* and *headreco* ($p = 0.19$) or between *mri2mesh* and the *fshires* ($p = 0.23$). The average percentage differences in the electric field over the 100 mm line for all subjects and target points are shown in Tables 1 and 2.

The average surface mappings for both the frontal and motor cortices are shown in Figs. 5 and 6. The average difference between the *headreco* and *mri2mesh* electric field results for the motor cortex are shown in Fig. 7. The electric fields and corresponding differences are mapped onto the *fsaverage* inflated surface along with cortical parcellation contours.

4 Discussion and Conclusion

This study focused on an evaluation of the electric field differences between The surface displacement between *mri2mesh* and *headreco* were seen at the CSF boundary, where the CSF surface was estimated closer to the gray matter for the *headreco* segmentation. Such surface displacement aligns with results shown in previous studies (cf., [11, 13]). In particular, Seiger et al. 2018 demonstrated that Freesurfer was more accurate in its calculation of cortical thickness; however, CAT12 based methods (such as *headreco*) were faster and yielded reliable results [16].

Differences between the *mri2mesh* and *fshires* were subtle as the underlying algorithm within FreeSurfer to segment the T_1 image is same for both methods. The lack of significant differences seen in the electric.

field between the two methods indicates that additional proceces to use a native submillimeter resolution is not necessary for BEM-FMM based computational modeling. Nevertheless, this may not be the case when highly detailed submillimeter surfaces are needed such as a very small structure.

In both the motor cortex and the DLPFC, the low average percent difference in the electric field suggests that the effect of the segmentation method differences was

Fig. 4 (continued) because they are almost identical to the *mri2mesh* results). Color indications for surfaces are red for skin, orange for skull, yellow for CSF, cyan for gray matter, and purple for white matter. The dotted white line on the axial cross section is a projection onto the XY plane of the 100 mm line running along the axis perpendicular from the coil. The electric field result along the dotted white line was extracted as shown at the bottom of the figure. The dotted black line indicates the location of the target point of stimulation. The field peaks were observed at the anatomical structure transition points (represented by arrows): (1) Skin-Skull, (2) Skull-CSF, (3) CSF-GM, (4) GM-WM

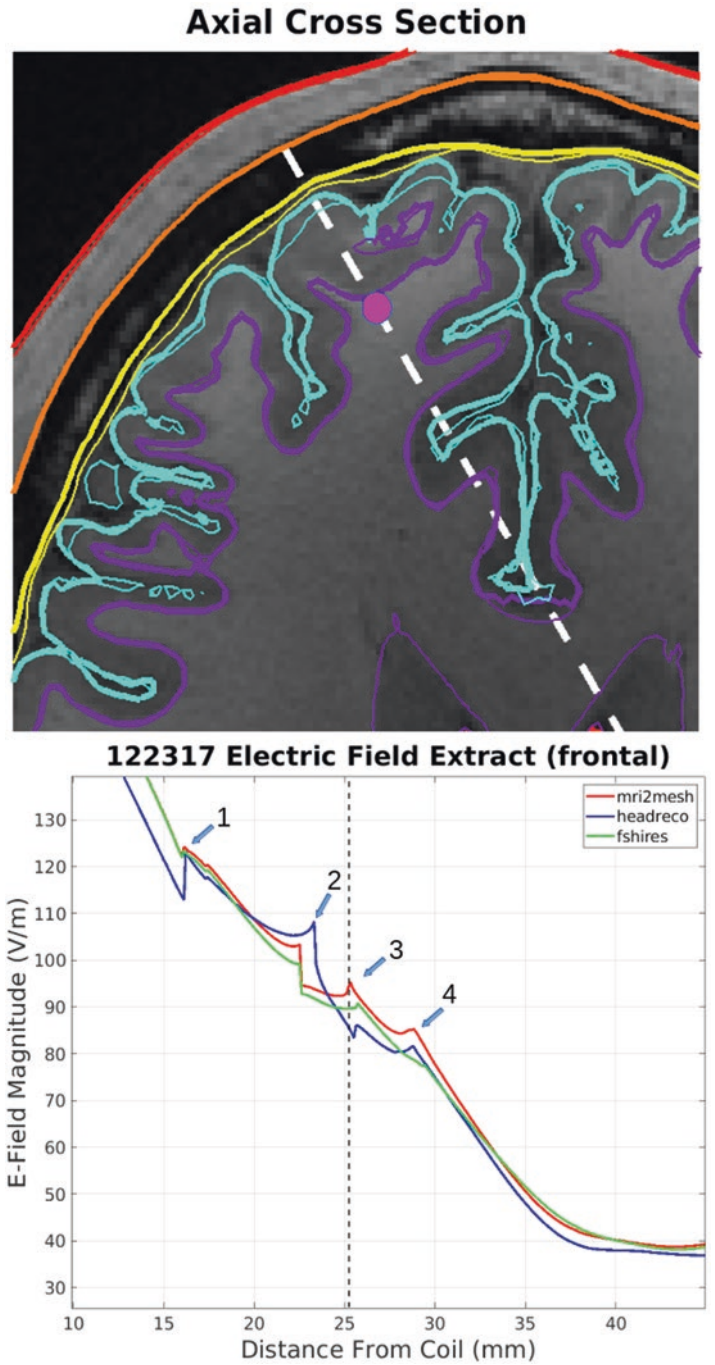

Fig. 4 Example of electric field targeted on DLPFC cortex is shown along with an axial cross section of a subject (target stimulation point in magenta). The thick contours show the *mri2mesh* field results and the thin contours show the *headreco* field results (*fshires* contours are not shown

Table 1 Average percentage difference between *mri2mesh* and *headreco* in the electric field magnitude for target points in the motor cortex and DLPFC for the 100 mm line and the average percentage difference in the region surrounding the target stimulation point (5 mm on either side of the line from the target point). Average percentage difference ranges from 82% to 112%

Subject	1	2	3	4	5	6	7	8	9	10	11	12	13	14	15	16
Motor (Obs line Avg)	1.02	0.98	1.00	1.03	0.96	0.97	0.97	0.95	0.99	1.04	1.01	0.97	0.99	0.92	0.99	0.94
Motor (target)	1.04	1.07	1.12	0.90	0.89	0.90	0.91	1.00	0.89	0.96	1.03	0.90	0.94	0.90	0.89	0.82
DLPFC (Obs line Avg)	0.97	1.08	1.07	0.95	1.03	1.00	1.01	1.08	1.12	1.04	1.04	1.06	1.01	1.03	0.99	0.96
DLPFC (target)	0.94	0.98	1.03	0.95	1.05	0.99	0.92	0.93	1.11	1.09	1.00	1.01	0.96	0.92	0.91	0.95

Table 2 Average percentage difference between *mri2mesh* and *fshires* in the electric field magnitude for target points in the motor cortex and DLPFC for the 100 mm line and the average percentage difference in the region surrounding the target stimulation point (5 mm on either side of the line from the target point). Average percentage difference ranges from 91% to 121%

Subject	1	2	3	4	5	6	7	8	9	10	11	12	13	14	15	16
Motor (Obs line Avg)	1.01	1.05	1.20	1.16	1.14	1.11	1.04	1.06	0.95	0.98	0.97	1.05	0.90	1.02	1.07	1.05
Motor (target)	0.96	0.97	1.02	1.06	1.03	1.04	1.00	1.00	1.00	0.96	0.99	1.04	0.96	0.97	1.02	0.96
DLPFC (Obs line Avg)	0.91	1.04	1.14	0.94	1.05	0.95	1.08	0.90	1.05	1.06	1.01	1.11	1.20	1.04	0.95	1.21
DLPFC (target)	0.99	1.00	1.05	0.99	1.03	0.98	0.98	1.00	1.02	1.01	0.99	1.00	0.96	0.97	0.98	0.95

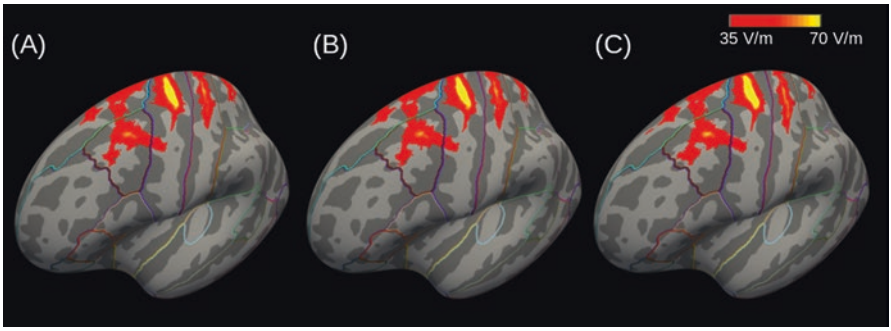

Fig. 5 Mean electric field values are mapped on the inflated surface for the motor cortex stimulation across all 16 subjects for *mri2mesh* (**a**), *fshires* (**b**), and *headreco* (**c**) along with the cortical parcellation contours. All three methods showed high electric field values in the target (precentral gyrus) along with the postcentral and caudal middle frontal gyri. No notable differences were observed between *fshires* and mri2mesh, and higher electric field values were observed in all three regions for the *headreco* method

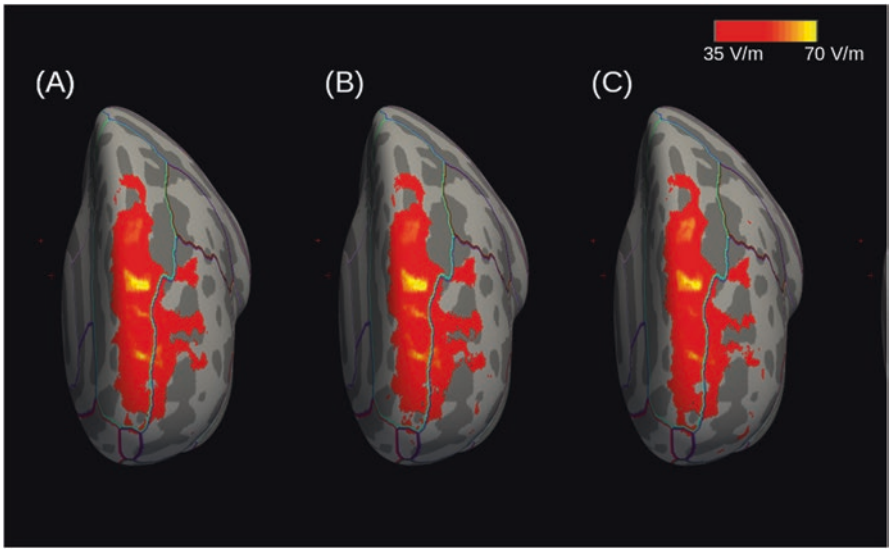

Fig. 6 Mean electric field values are mapped on the inflated surface for the DLPFC stimulation across all 16 subjects for *mri2mesh* (**a**), *fshires* (**b**), and *headreco* (**c**) along with the cortical parcellation contours. All three methods showed high electric field values in the target (superior frontal gyrus). No notable differences were observed between *fshires* and *mri2mesh*, and slightly lower electric fields were observed in all three regions for the *headreco* method

minimal. Although the overall difference was low (¡ 5%), the localized field difference near the target point across all 16 subjects was statistically significant for the motor cortex and could affect the intended stimulation there. The field difference for the DLPFC was not significant and the fields were more similar between *headreco* and *mri2mesh* as shown in Fig. 4.

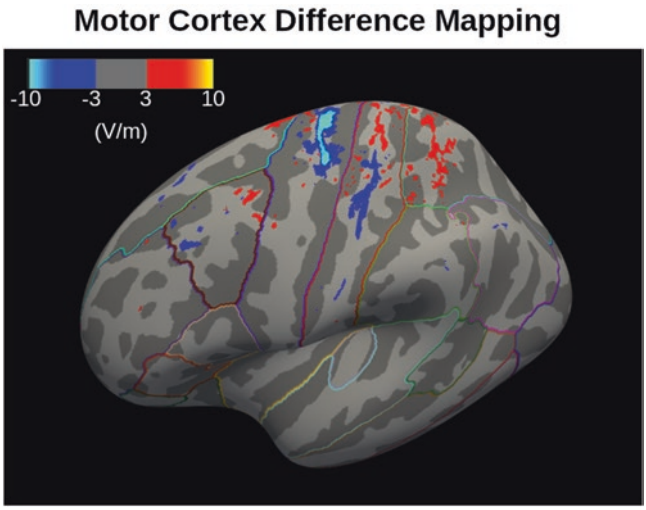

Fig. 7 Mean electric field differences between *mri2mesh* and *headreco* on the inflated surface are shown for the motor cortex stimulation. The area where the *headreco* electric field was lower than the *mri2mesh* electric field is shown in blue, and the area where the *headreco* electric field was higher than the *mri2mesh* electric field is shown in red

The percent difference in the electric field for the DLPFC was similar to that of the motor cortex along the entire 100 mm line for all 16 subjects. However, the region directly surrounding the target point showed lower variability for the DLPFC target compared to the motor cortex (Fig. 4). This trend is consistent in the average percent difference in the 5 mm region surrounding the target point. Therefore, there may be more segmentation variability in the motor cortex.

Analysis of the extracted electric field in Figs. 3 and 4 showed sudden changes in the field that resulted from the anatomical structure transitions. Some peaks are not aligned at the distance from the coil. For example, the Skull-CSF transitions in both figures were approximately 23 mm for the *headreco* segmentation whereas it was approximately 22.5 mm from the coil for the simulation with the *mri2mesh* and *fshires* methods. These sudden electric field changes resulting from segmentation differences can affect TMS therapy because the resulting neuronal excitation is a function of the electric field gradient rather than the electric field magnitude. Additional work that directly evaluates the gradient of the electric field will provide more insight into the effect of the segmentation on the TMS therapy.

The average electric field mapped on the *fsaverage* surface showed minimal differences between the *fshires* and *mri2mesh* segmentation methods as the differences were within 2 V/m. The electric field difference mapped on the *fsaverage* surface revealed that there were clusters that exceed 10 V/m of the electric field differences between *headreco* and *mri2mesh* (Fig. 7). The differences were also largely one-sided, with the fields from the *headreco* segmentation consistently higher than those from *mri2mesh*.

Coil positioning was critical to the electric field estimation. In this study, coil positioning was determined automatically based on the topology of the input meshes used. The pre-processing steps to select the proper coil position may differ significantly between segmentation methods.

The resulting field differences for each coil position were small but measurable. Though average percent differences observed along the 100 mm observation line were less than 5%, significant differences in the electric fields between segmentation methods were observed for the motor cortex simulation. Moreover, the field differences shown by subtle segmentation differences indicate an importance of patientspecific modeling as various previous studies have shown morphometric differences across age [14] and sex [17]. Future studies with different types of TMS coils and different segmentation and computational modeling methods may further improve a modeling approach for robust treatment for TMS and other neuromodulation devices.

Acknowledgments The authors would like to thank William Wartman for his assistance in visualizing the segmentations. The authors would also like to thank Drs. Brian B. Beard and Sunder S. Rajan for their helpful feedback.

Disclaimer The mention of commercial products, their sources, or their use in connection with the material reported herein is not to be construed as either an actual or implied endorsement of such products by the Department of Health and Human Services.

References

1. J. Ashburner, K. Friston, Image segmentation, in *Human Brain Function*, ed. by R. Frackowiak, K. Friston, C. Frith, R. Dolan, K. Friston, C. Price, S. Zeki, J. Ashburner, W. Penny, 2nd edn., (Academic Press, 2003), Headquartered in Cambridge, Massachusetts
2. A.M. Dale, B. Fischl, M.I. Sereno, Cortical surface-based analysis: I. Segmentation and surface reconstruction. *Neuroimage* **9**(2), 179–194 (1999)
3. R. Dubbioso, E. Raffin, A. Karabanov, A. Thielscher, H.R. Siebner, Centre-surround organization of fast sensorimotor integration in human motor hand area. NeuroImage **158**, 37–47 (2017)
4. B. Fischl, M.I. Sereno, A.M. Dale, Cortical surface-based analysis: II: inflation, flattening, and a surface-based coordinate system. NeuroImage **9**(2), 195–207 (1999)
5. M.I. Iacono, E. Neufeld, E. Akinnagbe, K. Bower, J. Wolf, I.V. Oikonomidis, D. Sharma, B. Lloyd, B.J. Wilm, M. Wyss, et al., MIDA: a multimodal imaging-based detailed anatomical model of the human head and neck. PLOS One **10**(4), e0124126 (2015)
6. K. Kazemi, N. Noorizadeh, Quantitative comparison of SPM, FSL, and brainsuite for brain MR image segmentation. J. Biomed. Phys. Eng. **4**(1), 13 (2014)
7. S. Makarov, W. Wartman, G. Noetscher, K. Fujimoto, T. Zaidi, E. Burnham, M. Daneshzand, A. Nummenmaa, Degree of improving tms focality through a geometrically stable solution of an inverse tms problem. NeuroImage **241**, 118437 (2021)
8. S.N. Makarov, G.M. Noetscher, T. Raij, A. Nummenmaa, A quasi-static boundary element approach with fast multipole acceleration for high-resolution bioelectromagnetic models. IEEE Trans. Bio-med. Eng. **65**(12), 2675–2683 (2018)
9. S.N. Makarov, W.A. Wartman, M. Daneshzand, K. Fujimoto, T. Raij, A. Nummenmaa, A software toolkit for TMS electric-field modeling with boundary element fast multipole method: an efficient MATLAB implementation. J. Neural Eng. **17**(4), 046023 (2020)

10. J.D. Nielsen, K.H. Madsen, O. Puonti, H.R. Siebner, C. Bauer, C.G. Madsen, G.B. Saturnino, A. Thielscher, Automatic skull segmentation from MR images for realistic volume conductor models of the head: assessment of the state-of-the-art. NeuroImage **174**, 587–598 (2018)
11. O. Puonti, G.B. Saturnino, K.H. Madsen, A. Thielscher, Value and limitations of intracranial recordings for validating electric field modeling for transcranial brain stimulation. NeuroImage **208**, 116431 (2020)
12. E. Raffin, G. Pellegrino, V. Di Lazzaro, A. Thielscher, H.R. Siebner, Bringing transcranial mapping into shape: sulcus-aligned mapping captures motor somatotopy in human primary motor hand area. NeuroImage **120**, 164–175 (2015)
13. R. Righart, P. Schmidt, R. Dahnke, V. Biberacher, A. Beer, D. Buck, B. Hemmer, J. Kirschke, C. Zimmer, C. Gaser, et al., Volume versus surface-based cortical thickness measurements: a comparative study with healthy controls and multiple sclerosis patients. PLOS One **12**(7), e0179590 (2017)
14. D.H. Salat, R.L. Buckner, A.Z. Snyder, D.N. Greve, R.S. Desikan, E. Busa, J.C. Morris, A.M. Dale, B. Fischl, Thinning of the cerebral cortex in aging. Cereb. Cortex **14**(7), 721–730 (2004)
15. G. Saturnino, A. Antunes, J. Stelzer, A. Thielscher. Simnibs: a versatile toolbox for simulating fields generated by transcranial brain stimulation. In *21st Annual Meeting of the Organization for Human Brain Mapping (OHBM 2015)*, 2015
16. R. Seiger, S. Ganger, G.S. Kranz, A. Hahn, R. Lanzenberger, Cortical thickness estimations of FreeSurfer and the CAT12 toolbox in patients with Alzheimer's disease and healthy controls. J. Neuroimaging **28**(5), 515–523 (2018)
17. E.R. Sowell, B.S. Peterson, E. Kan, R.P. Woods, J. Yoshii, R. Bansal, D. Xu, H. Zhu, P.M. Thompson, A.W. Toga, Sex differences in cortical thickness mapped in 176 healthy individuals between 7 and 87 years of age. Cereb. Cortex **17**(7), 1550–1560 (2007)
18. D.L. Tudorascu, H.T. Karim, J.M. Maronge, L. Alhilali, S. Fakhran, H.J. Aizenstein, J. Muschelli, C.M. Crainiceanu, Reproducibility and bias in healthy brain segmentation: comparison of two popular neuroimaging platforms. Front. Neurosci. **10**, 503 (2016)
19. D.C. Van Essen, K. Ugurbil, E. Auerbach, D. Barch, T.E. Behrens, R. Bucholz, A. Chang, L. Chen, M. Corbetta, S.W. Curtiss, et al., The human connectome project: a data acquisition perspective. NeuroImage **62**(4), 2222–2231 (2012)
20. M. Windhoff, A. Opitz, A. Thielscher. *Electric Field Calculations in Brain Stimulation Based on Finite Elements: An Optimized Processing Pipeline for the Generation and Usage of Accurate Individual Head Models*. Technical report, Wiley Online Library, 2013
21. N. Zaretskaya, B.R. Fischl, M. Reuter, V. Renvall, J. Polimeni, Advantages of cortical surface reconstruction using submillimeter 7 t memprage. NeuroImage **165**, 11–26 (2018)
22. Y. Zhang, M. Brady, S. Smith, Segmentation of brain MR images through a hidden Markov random field model and the expectation-maximization algorithm. IEEE Trans. Med. Imaging **20**(1), 45–57 (2001)